TIME-DEPENDENT PHASE SPACE MEASUREMENTS OF THE LONGITUDINALLY COMPRESSING BEAM IN NDCX-I*

S.M. Lidia#, G. Bazouin, P.A. Seidl, LBNL, Berkeley, CA 94720, U.S.A

Abstract

The Neutralized Drift Compression Experiment (NDCX-I) [1] generates high intensity ion beams to explore Warm Dense Matter physics. A ~150 kV, ~500 ns modulating voltage pulse is applied to a ~300 kV, 5-10 μs, 25 mA K+ ion beam across a single induction gap. The velocity modulated beam compresses longitudinally during ballistic transport along a space charge neutralizing plasma transport line, resulting in ~3A peak current with ~2-3 ns pulse durations (FWHM) at the target plane. Transverse final focusing is accomplished with a ~8 T, 10 cm long pulsed solenoid magnet. Time-dependent electrostatic focusing in the induction gap, and chromatic aberrations in the final focus optics limit the peak fluence at the target plane for the compressed beam pulse. We report on time-dependent phase space measurements of the compressed pulse in the ballistic transport beamline, and measurement of the time-dependent radial impulses derived from the interaction of the beam and the induction gap voltage. We present results of start-to-end simulations to benchmark the experiments. Fast correction strategies are discussed with application to both NDCX-I and the soon to be commissioned NDCX-II [2] accelerators.

NDCX-I EXPERIMENT

The goal of the NDCX-I and NDCX-II facilities is to produce and direct high fluence ion beams onto material targets that quickly drive the target material into the 'warm dense matter' regime [3]. The operating principal in these devices is to create a 'velocity tilt' on the beam by applying a time-varying energy modulation, and then allow for high longitudinal compression in a plasma-neutralized drift beamline prior to final focusing onto the target. With sufficiently high plasma densities, emittance-dominated transport is achieved and the ion beam density is increased by several orders of magnitude over that of the space-charge limited ion beam source. The NDCX-I beamline is shown in Fig. 1 below.

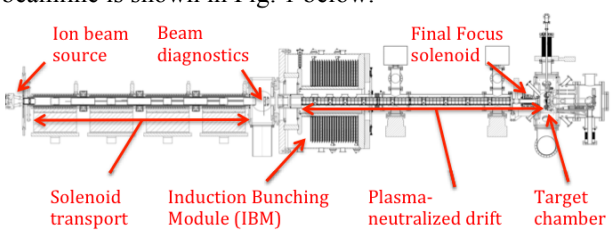

Figure 1: NDCX-I facility 6-meter long beamline.

The initial acceleration and extraction in performed with an ion source and Marx column to produce the beam. Four solenoid magnets and three x/y dipole magnet pairs transport the beam from the source, through the Induction Bunching Module (IBM, and into the plasma-neutralized drift section. The final focus magnet is the final optic to control the beam fluence on target. The beam divergence angle onto the target is ~80 mrad. Not shown are the several biased-cylinder (~3 kV) electron traps along the vacuum beamline that hinder the flow of secondary electrons that might otherwise disrupt the ion beam transport, and a vertically-polarized pair of magnetic dipoles (~900 G peak field, +- axial layout to null the on-axis field integral) immediately upstream of the plasma channel to assist in removing backstreaming electrons.

Longitudinal Compression

The IBM voltage waveform is synthesized and tuned for different injector beam energies to optimally velocity-modulate and compress the beam at the target plane. The compressed and uncompressed beam current profiles at the target plane are shown in Fig. 2. The rarefied and intensified regions are clearly identified. Fig. 3 shows detail of the compressed pulse region. The peak current has increased by ~90X that of the uncompressed current.

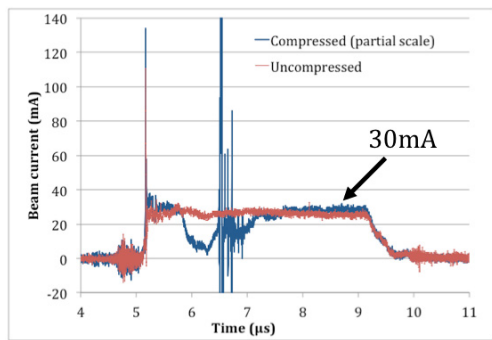

Figure 2: Compressed and uncompressed beam current at the target plane.

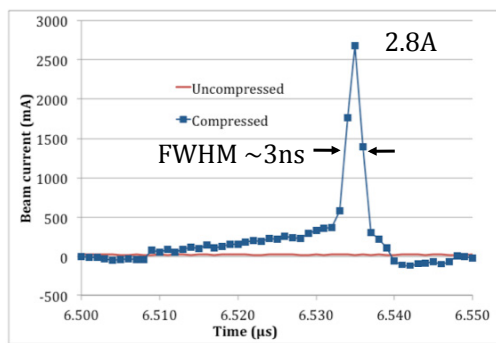

Figure 3: Detail of compressed pulse current profile.

*Work supported by U.S. Department of Energy under Contract No. DE-AC02-05CH11231.
#smlidia@lbl.gov

Fluence-limiting Aberrations

The beam fluence is measured at the target plane using an alumina scintillator and a gated, image-intensified microchannel plate camera, cross-calibrated against a fast (~1 ns resolution) Faraday cup. Fluence maps for the uncompressed and compressed beams are shown in Fig. 4. Finite emittance, and chromatic and geometric aberrations reduce the peak compressed-to-uncompressed fluence ratio from that of the peak current compression ratio. Chromatic aberrations in the NDCX-I modulated beam introduce a 'circle of confusion' with radius ~5 mm. Time-varying electric gap fields, like those found in the IBM, produce both a focusing and a defocusing effect on the beam, altering the beam slice transport to the final focus.

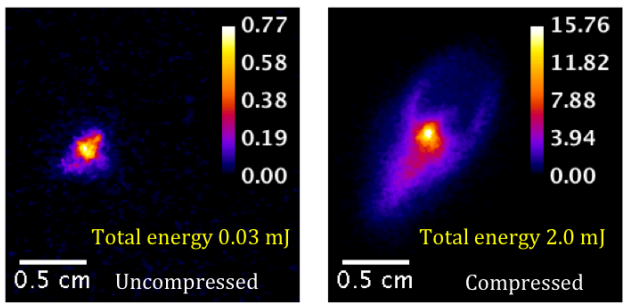

Figure 4: Target plane beam fluences in a 3.5ns window on the uncompressed and compressed beam.

MEASURING THE MODULATED BEAM PHASE-SPACE

Facility beamline design improvements to increase the peak on-target beam fluence have so far concentrated on 'fast' correction schemes [4]. Additional beamline elements, such as a pulsed Einzel lens, can produce time-varying changes in the beam envelope that may partially compensate for time-varying focusing variations induced by the IBM itself. Measuring the temporal variation of the modulated and compressing beam pulse can indicate the amplitude and time rate of change of needed focusing variations. To temporally resolve the modulated beam phase space variations, a shortened drift line was required so that the compressed pulse region still carried a pulse width (FWHM) of several hundred nanoseconds.

Modified NDCX-I Experiment

The NDCX-I beamline was altered to insert a beam diagnostic suite immediately downstream from the IBM. Two diagnostic chambers ('Box 1' and 'Box 2') are used to fully characterize the beam current, spatial profile, and time-resolved phase space density before and after modulation. Spatial constraints dictated that the downstream diagnostic chamber be placed ~1.75 m from the IBM gap, and to include ~1.2 m of neutralizing plasma transport line. An electron trap was inserted at the Box 2 entrance to separate the plasma-filled beam tune from the vacuum diagnostic chamber. The modified beamline is shown schematically in Fig. 5.

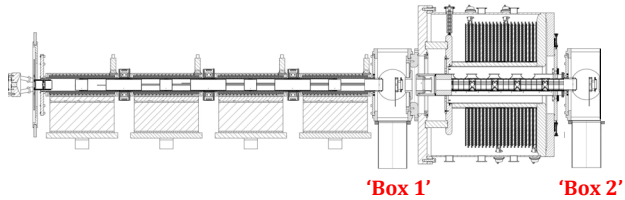

Figure 5: Modified NDCX-I beamline, showing the location of the beam diagnostic chambers.

Data Acquisition and Processing

The beam phase space density was measured with horizontal and vertical slit and slit Faraday cup devices. Beam profile was measured with both optical scintillators and gated cameras, and with the horizontal and vertical slit Faraday cups. Beam current was measured with deep (10 cm) Faraday cups. The Faraday cup signals were acquired with a Tektronix TDS 654C 500MHz sampling oscilloscope to provide ~1 ns temporal resolution. Signals were archived and batch processed in software after measurement scans concluded. The slit-slit cup separation is ~10 cm. The step size of the slit and slit cup position scan was 0.1 mm, resulting in an angular resolution of ~1 mr. Timing and synchronization of the various Faraday cup signals was performed by aligning the beam pulse rise and fall times. This procedure allows for the unambiguous comparison of phase space density profiles between the uncompressed and compressed beams in both horizontal and vertical scans.

Time-resolved Beam Envelope Variations

The results of the deep Faraday cup and slit-slit Faraday cup scans are shown in Figs. 6-9. The time coordinate shown is the delay from the beam pulse head arrival time. The beam modulation results in partial longitudinal compression and some current amplification. The current measurement (Fig. 6) in Box 2 shows the modulated region to occur in the interval $0.9\ \mu s < t < 1.5\ \mu s$.

The measured beam emittance (Fig. 7) of the modulated beam shows significant (~20%) temporal variation in the modulated region, indicating nonlinear forces in the beam transport. Also evident is the difference in variation between the horizontal and vertical planes, indicating a possible breakdown in axial symmetry. This may indicate time-varying coupling between the modulated beam and the weak magnetic dipoles.

The beam envelope (Fig. 8) and divergence angle (Fig. 9) also show similar variation along the compressed region. The unmodulated beam current, emittance, and beam envelope show insignificant variation over the same region. The unmodulated beam divergence angle does show significant evolution of the time interval, indicating possible electron or instrumental effects. Similar background variation is also evident in the modulated beam divergence angle measurement, in addition to the variation due to the modulation itself (Fig. 9).

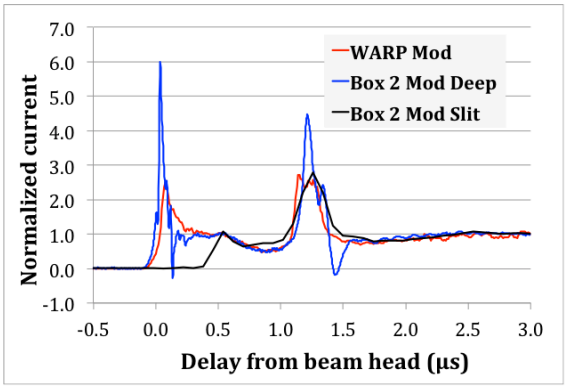

Figure 6: Comparison of the normalized current measurements of the modulated beam.

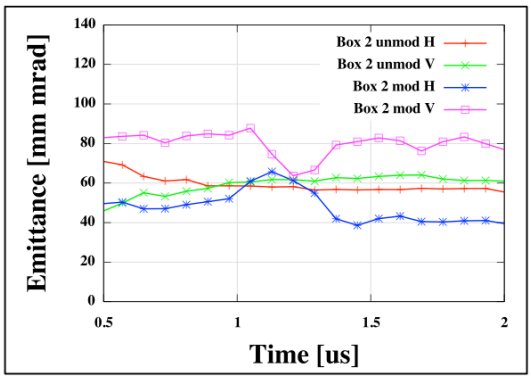

Figure 7: 4*rms emittance measurements of modulated ('Mod') and unmodulated ('Unmod') beam.

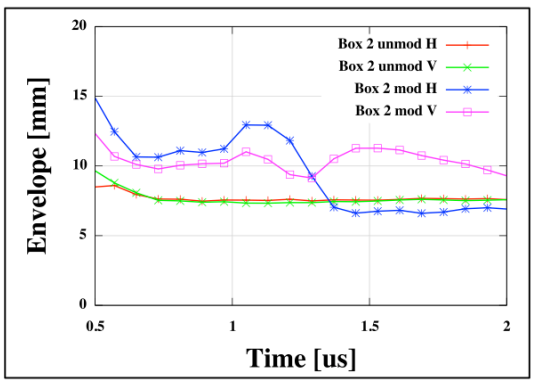

Figure 8: Envelope radius (2*rms) measurements of modulated ('Mod') and unmodulated ('Unmod') beam.

Model Comparison

An axisymmetric WARP [5] model was created to perform high-resolution particle-in-cell modeling. The plasma has been included as an ideal neutralizing background, without dynamical variations. WARP results are shown in Fig. 10. The 4*rms beam emittance, not shown, remains constant at ~30 mm-mrad. The evolution of the beam envelope and the envelope divergence angle remain consistent with linear optics.

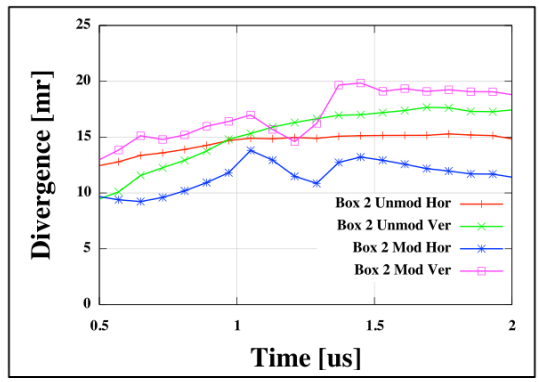

Figure 9: Envelope divergence angle measurements of modulated ('Mod') and unmodulated ('Unmod') beam.

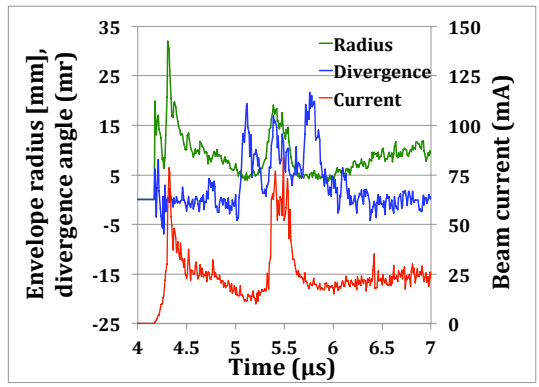

Figure 10: Axisymmetric WARP model results in Box 2. Difference in the beam envelope and divergence between the modulated and unmodulated beams are shown.

CONCLUSIONS

We have made a series of time-resolved measurements of the beam parameters and phase space density of an intense, velocity-modulated ion beam transported through a plasma-neutralized channel. Measurements indicate significant deviations from linear behavior in axisymmetric transport channels. Possible mechanisms for emittance variations in the modulated beam may include large scale 3D density perturbations in the space charge dominated beam, coupling to weak magnetic chicanes, and electron trap bias deviations resulting in backstreaming electron flows.

REFERENCES

[1] P.A. Seidl, *et al*., Proceedings of the 2009 Particle Accelerator Conference, TH3GAI04.
[2] A. Friedman, *et al*., NIM A **606** (2009), 6-10.
[3] F.M. Bieniosek, *et al.,* 2010 *J. Phys.: Conf. Ser.* **244** 032028.
[4] S. Lidia, *et al*., Proceedings of the 2009 Particle Accelerator Conference, TU6PFP093.
[5] A. Friedman, *et al*., *Phys. Fluids B* **4** (1992), 2203.